NANO LETTERS

Letter

pubs.acs.org/NanoLett

Resolving Voltage–Time Dilemma Using an Atomic-Scale Lever of Subpicosecond Electron–Phonon Interaction

Xiang Yang, Ioan Tudosa, Byung Joon Choi, Albert B. K. Chen, and I-Wei Chen*

Department of Materials Science and Engineering, University of Pennsylvania, Philadelphia, Pennsylvania 19104-6272, United States

Supporting Information

ABSTRACT: Nanoelectronic memory based on trapped charge need to be small and fast, but fundamentally it faces a voltage–time dilemma because the requirement of a high-energy barrier for data retention under zero/low electrical stimuli is incompatible with the demand of a low-energy barrier for fast switching under a modest programming voltage. One solution is to embed an atomic-level lever of localized electron–phonon interaction to autonomously reconfigure trap-site's barrier in accordance to the electron-occupancy of the site. Here we demonstrate an atomically levered resistance-switching memory built on locally flexible amorphous nanometallic thin films: charge detrapping can be triggered by a mechanical force, the fastest one being a plasmonic Lorentz force induced by a nearby electron or positron bunch passing in 10^{-13} s. The observation provided the first real-time evidence of an electron–phonon interaction in action, which enables nanometallic memory to turn on at a subpicosecond speed yet retain long-term memory, thus suitable for universal memory and other nanoelectron applications.

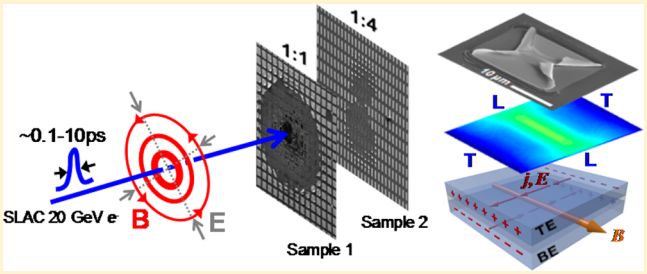

KEYWORDS: *Resistive switching memory, amorphous materials, metal insulator transition, electron–phonon interaction, plasmonic, pressure (effect)*

Itinerant electrons in random materials with intrinsic underlying disorder are random waves with a localization length ζ.[1,2] Size is thus critical because the wave functions extended beyond ζ decay exponentially. This naturally leads to a size-dependent metal–insulator transition (MIT):[3−5] when one or more of the dimensions (e.g., film thickness δ) of a random insulator fall below ζ, random waves can reach across the sample in the corresponding direction; thus the sample behaves like a metal—a *nanometal*. Active stimuli control can be achieved by injecting, and later extracting, extrinsic disorder. As ζ is first reduced, then restored, a reversible MIT follows.[3,4] Another consequence of random atomic structure is that it contains locally soft atomic spots with localized atomic forces.[6] This paper will demonstrate that such electronic and mechanical attributes make amorphous films an ideal electron-trapping, resistance-switching nano platform that defies the voltage–time dilemma,[7−9] capable of long-term memory and an ultrafast programming speed.

Voltage-controlled nanometallic memory has been implemented in amorphous films mixing insulators (SiO_2 or Si_3N_4) and metals (Pt or Cr).[3,10,11] At a threshold bias voltage V^*, some electrons crossing the film become trapped, erecting Coulomb repulsion as random fields. This reduces ζ by ∼10 times,[4] rendering the film insulating. Detrapping by applying an opposite bias $-V^*$, or by UV irradiation without any voltage, returns the film to the metallic state. As the temperature approaches 0 K, the two states exhibit metallic and insulating characteristics, respectively: decreasing resistance for the low-resistance-state (LRS or ON-state) versus diverging resistance for the high-resistance-state (HRS or OFF-state). Intermediate states are also accessible by voltage control, which tunes the amount of residual trapped electrons.[3]

Scalable internal-resistance memory utilizing nanometallic MIT already exhibits excellent uniformity, durability, retention life of at least several years, and <100 ps switching speed,[4,11,12] which prompts the question why this electronic memory has apparently escaped the voltage–time dilemma.[7−9] Theoretically, no energy barrier (having *two* independent characteristics or variables: barrier height and width) that separates a trapped-charge-state from a free-charge-state can simultaneously satisfy *three* specifications: the programming voltage, programming time/speed and retention time.[4,7−9,13,14] Moreover, since the trapped-electron-state often experiences an on-site Coulomb repulsion (the Hubbard U), the positive-U electron sees a lowered barrier making the state even less capable of retaining memory. Our study aims to fundamentally resolve this seemingly intractable problem that has troubled the electronic community. By probing the energetics and subpicosecond dynamics of MIT in nanometallic amorphous films, it reveals the existence of an electron–phonon interaction that can reconfigure the trapped-charge-state, from an unstable positive-U state to a stable negative-U state, and vice versa. In this way,

Received: May 7, 2014
Revised: August 1, 2014
Published: August 5, 2014

ACS Publications © 2014 American Chemical Society

the barrier height becomes adjustable, and the barrier has more than two variables, so there is no dilemma! It also finds V^* an essentially invariant property in a wide range of nanometallics (Table 1) with various nanostructures and compositions, which confers simplicity and flexibility to CMOS design and manufacturing.

Table 1. Atomic Insulator:Metal Hybrids Exhibiting Nanometallic Transitions and Switching Behavior[a]

insulator:metal	insulator:metal
SiO_2:Pt	AlN:Pt
MgO:Pt	Si_3N_4:Al
Al_2O_3:Pt	Si_3N_4:Cr
Y_2O_3:Pt	Si_3N_4:Cu
HfO_2:Pt	Si_3N_4:Ta
Ta_2O_5:Pt	Si_3N_4:Pt
SiO_xN_y:Pt	

[a] Si_3N_4:Pt/Cr, and SiO_2:Pt systems are from refs 3−5, 10, 11, and 62.

We first outline a detailed study of our devices to ascertain their electronic nature of switching. Depending on the thickness δ and metal fraction f, a random insulator:metal film tested between two *different*-metal electrodes (Figure 1a) can be a metal or an insulator, or switch between the two via a hysteretic, voltage-controlled MIT. The conduction status of the films, summarized in δ-f maps[3] (one in Figure 1b), was determined for all the systems in Table 1, which exhibit universally similar switching curves (Supporting Information, Figure S1) as the ones in Figure 1b. Structurally, all switchable films appeared amorphous to conventional X-ray diffraction (Supporting Information, Figure S2), but their TEM nanostructures ranged from ones with a worm-like contrast (typical for amorphous networks)[3] without any resolvable inclusion (Figure 1c, upper panel) to ones with metal-rich inclusions (dark regions in Figure 1c, lower panel) embedded in a similarly amorphous background. Therefore, switching occurs with or without metal-rich clusters. This was confirmed by the switching resistance (R)-voltage (V) curves for a wide range of nanostructures in the Supporting Information, Figure S3, including ones with a metal fraction at one-tenth of the cluster-percolation threshold.[3] Thus, unlike metal-nanocrystal memory, which stores electrons in discrete metal nanodots (e.g., Au and Pt in SiO_2[8,9,15]), in our devices isolated metal-rich clusters are mere spectators of nanometallic MIT. Random-wave electrons must have come from the random network itself, most likely from the electron-rich metal atoms/oligomers dispersed on the three-dimensional insulator scaffold. (When specialized to two dimensions, metal atoms randomly residing in an immiscible insulator have a configuration akin to random metal atoms on a catalytic support, such as Al_2O_3 and SiO_2.)

With few exceptions,[16−21] widely reported resistance-switching films all operate on ion-motion mechanisms.[22−25] Their electrode−film interface sometimes plays an important role as evident from their asymmetric or rectifying R−V and current (I)−V curves.[22] Such features are absent in Figure 1b and d, which are Ohmic when <0.1 V and remain polarity-symmetric below ∼1 V, even though the devices are asymmetrically structured having two metal electrodes of different work functions (Figure 1a). (Usually, our top electrode has a higher work function than the lower electrode.) This is consistent with the completely polarity-symmetric capacitance−voltage curve in Figure 1e, indicating lack of a Schottky barrier. The I−V curves for ion-motion mechanisms often show a voltage offset at zero current, reflecting the gradient of the internal ion potential that is too slow to equilibrate with the sweeping drive-voltage.[26] Again, this feature is absent in nanometallic devices at the nA−mV resolution (Figure 1d inset). Along with the finding that UV, which cannot motivate ion motion but can trigger insulator→ metal switching without applying a voltage (Supporting Information, Figure S4a−c),[3] these observations ruled out ion-current's participation in nanometallic MIT.

Our switching device is thus a purely electronic one relying on electron trapping/detrapping within the disordered film to regulate ζ and effect MIT, with rather uniform properties (Figure S4d−e). In ordinary MIT, whether the ground state is metallic or insulating is field (temperature, stress, electric/magnetic) dependent: both are possible as evidenced by field-induced two-way metal↔insulator conversions.[27,28] In nanometallic MIT, however, the insulating state (HRS) shares with the metallic state (LRS) a structurally identical bulk state except

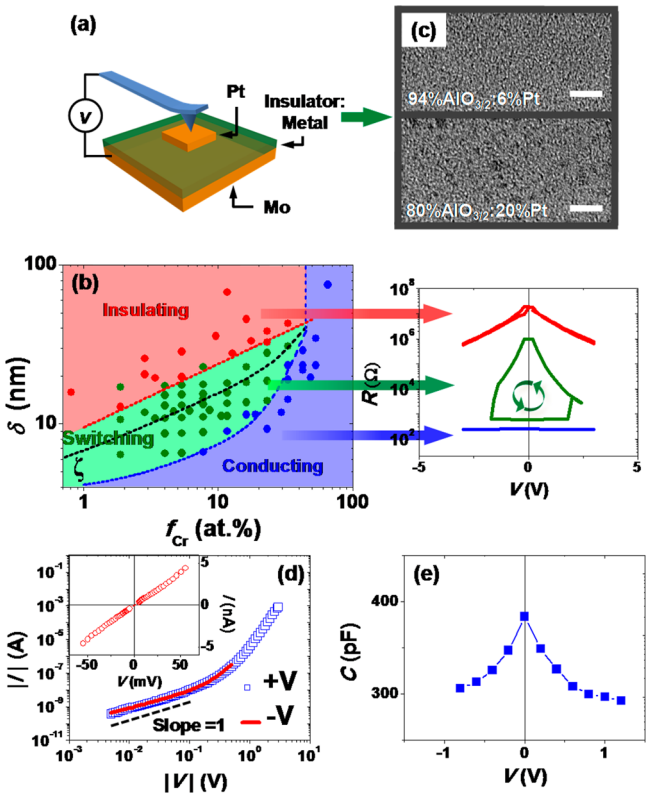

Figure 1. Nanometallic MIT. (a) Configuration of asymmetric test device; unless otherwise noted, top electrode metal has a larger work function (e.g., Pt) than bottom electrode metal (e.g., Mo). (b) δ-f map for $(1-f)$ $SiN_{4/3}$:f Cr films sandwiched between Pt and Mo delineating data points for insulating, conducting and switching behavior, with corresponding representative resistance (R) vs voltage (V) curves, showing percolation at metal composition f = 0.45, nanometallicity at thinner thickness from $f \sim 0$ to $f = 0.45$, and switching when thickness $\delta \approx \zeta$, the latter as black dotted curve. During switching, an initially conducting film transitions to high-resistance insulating state at +2 V and returns to low-resistance metallic state at −1.5 V. Cell diameter: 200 μm. (c) Plan-view transmission electron microscopy (TEM) images (bright field) of 94% $AlO_{3/2}$:6%Pt (top) and 80%$AlO_{3/2}$:20%Pt (bottom) films. Scale bar: 5 nm. (d) HRS I−V curves in log−log scale with overlapping data under positive (+) and negative (−) polarities, following $I \sim V$ at small V. Inset: Enlarged I−V curve in the nA range illustrating linear I−V crossing origin. (e) Symmetric capacitance (C)−V curves for HRS.

dx.doi.org/10.1021/nl501710r | Nano Lett. 2014, 14, 5058−5067

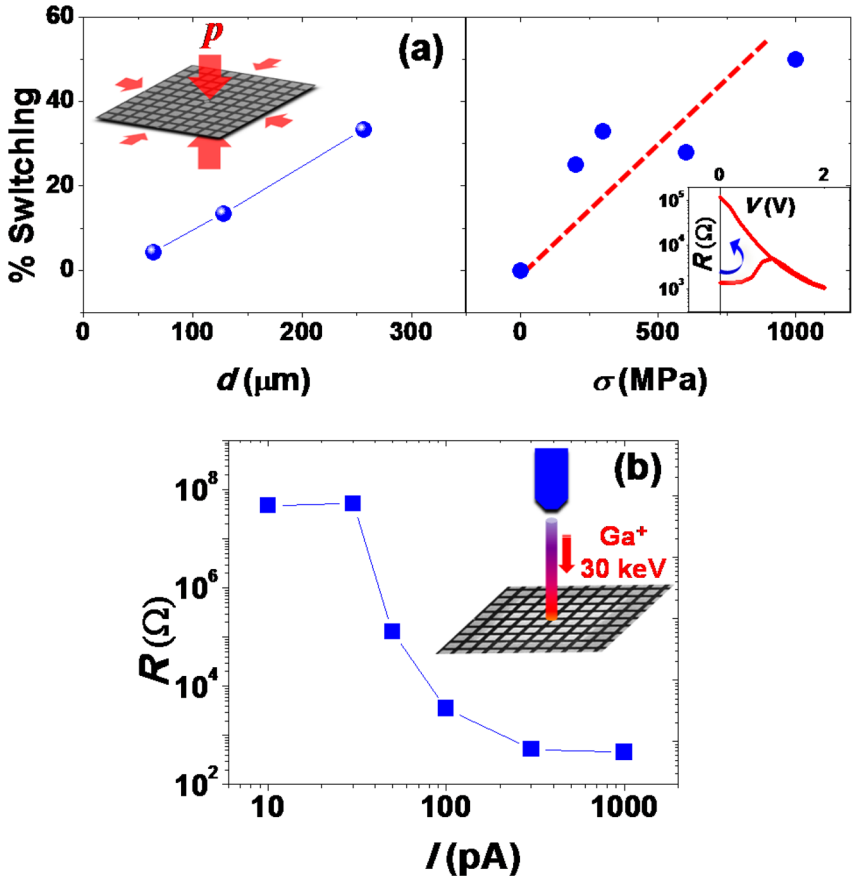

Figure 2. Mechanically induced MIT. (a) Schematic of isostatic pressure and percentage of LRS cells after pressure treatment as a function of device size (fixed 300 MPa pressure) and applied pressure (fixed device size 256 μm). All devices preset to HRS. Inset: $R-V$ characteristics of pressure-switched device switching back to HRS under positive voltage. (b) Schematic of Ga^+ bombardment and HRS resistance after 20 s bombardment by 30 keV Ga^+ ions of various currents. Switching to intermediate states starts at >50 pA, becoming nearly complete at 300 pA. All retain switching capability as shown in the Supporting Information, Figure S6f–g. With a maximum range of 13.2 nm in Pt (see range calculation in Figure S5a), 30 keV Ga^+ is completely stopped in the top electrode, 40 nm Pt.

for the additional localized electronic/structural disorders that arise from the trapped charge. The experiments below establish such localized states, at zero voltage, are metastable: a sufficiently large mechanical perturbation, static or subpicosecond one, can destabilize them to detrap electrons. This triggers a one-way HRS→LRS transition that is not reversed when the perturbations is removed or reversed. Mechanically induced electron detrapping is a testament of reconfigurable barriers and electron–phonon interaction. Thus, the experiments also resolve the voltage–time dilemma.

Our first perturbation was a uniform (isostatic) pressure of 300 MPa (Figure2a, left panel) or other values (Figure 2a, right panel) applied to all the devices on a chip inside a hydraulic pressure vessel. Postpressurization measurements found that, with increasing device sizes and pressure, an increasing percentage of HRS devices had switched to LRS (Figure 2a). The pressure-induced switching was nondamaging: in subsequent testing the devices repeatedly switched in either direction with the same characteristic $R-V$ curves as before (Figure 2a inset). But unlike two-way switching under a voltage trigger, pressure only induced one-way switching: no LRS→HRS switching was found at all. Therefore, the HRS is metastable, which irreversibly transitions to the LRS, the ground state, under large perturbations.

Since there was no voltage to drive ion motion and a uniform pressure cannot move ions either, pressure-induced switching must be due to electron detrapping. Without any electrical force, what a mechanical force can do at most is to rearrange the atomic structure (e.g., relative atomic displacement and bond distortion), which is apparently sufficient to cause spontaneous detrapping. Therefore, a reduction of barrier height of the reconfigured barrier must have happened. (The reconfiguration is reversible, since the device was not damaged.) The above experiment thus established the reconfigurability of the barrier, which fundamentally removes the voltage–time dilemma.

But can electron detrapping be induced by mere 300 MPa—well below the critical pressure (~3–30 GPa) typical for electronic transitions, given the estimated strain of only <0.2%? (We used a Young's modulus of 100 GPa and a Poisson's ratio of 0.2, typical for amorphous Si_3N_4 films, for the estimate.) The answer lies in the fact that amorphous materials are not elastically uniform: they contain locally soft atomic spots[6] which may buckle under a modest pressure. These spots can provide the sites for electron trapping and detrapping. Previously, to explain the apparent retention stability of nanometallic HRS during storage, we already proposed that the energy barrier at the trap site can be reconfigured by localized electron–phonon interaction. Specifically, it drives bond distortion to reduce the energy of a freshly trapped electron by ϕ_{ep}, turning it into a stable negative-U state; conversely, an opposite bond distortion unravels ϕ_{ep}, restoring

dx.doi.org/10.1021/nl501710r | Nano Lett. 2014, 14, 5058–5067

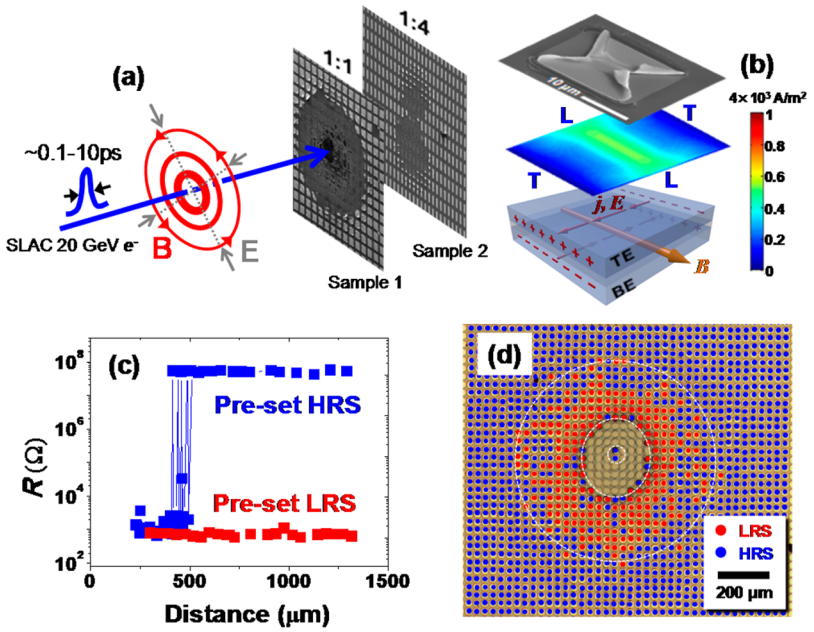

Figure 3. Subpicosecond switching. (a) A single shot of relativistic electron bunch hitting the sample with the cell array. Also shown are the electric field and magnetic induction. (For the positron bunch, the field directions are reversed.) One experiment used sample 1 with 20 μm square devices, and the other used sample 2 with high-aspect-ratio (1:4) rectangular devices. (b) Top panel: top Pt electrode of square device deformed into "bow-tie," viewed at an angle; middle: simulated current density distribution in top electrode; bottom: incoming magnetic field B and induced current j, electric field E, and charge in schematic device with top electrode (TE) and bottom electrode (BE) separated by an insulator gap. (c) In sample 1 (TE thickness: 40 nm), devices preset to HRS switched to LRS if located within ~450 μm from hit-spot; devices preset to LRS remained in LRS at all distance. Devices within 200 μm lost the top electrodes completely and were not tested. (d) Optical image of circular (20 μm) devices with thicker (100 nm) TE preset to HRS. Added colors indicate different states after experiment, blue: HRS; red: LRS; yellow: top electrode torn away. Drawn circles going outward indicate four zones of different device states, starting from (no damage & HRS)→ (top electrode torn away) → LRS → HRS.

the positive-U state of the trapped electron, which prompts it to detrap.[4,11] The pressure experiment unequivocally confirmed two key elements expected of the above mechanism: the action of electron−phonon interaction must entail (a) a strain via bond distortion (thus a stress can unravel ϕ_{ep}) and (b) electron occupancy (thus a stress can induce detrapping but not trapping).

To corroborate the static experiment, a quasi-static mechanical perturbation was next provided by beams of 30 keV Ga^+ ions and electrons (Figure 2b and Figure S6). Via momentum transfer (Figure S6), they exert a compressive pressure given by $j(2mK)^{1/2}/e$, where j and m are, respectively, the current density and mass of Ga^+ or electron, K = beam energy (30 keV) and e is the elementary charge. As the beam in a Gaussian size of 3 nm scanned a ~15 × 12 μm^2 area (Supporting Information, Figure S6a−d) on an HRS device (20 μm wide) in 20 s, it spent ~1 μs at every point. Ex situ measured resistance (Figure 2b) showed a resistance drop beginning with 50 pA bombardment; 300 pA bombardment caused a drop comparable to that of a typical voltage-triggered HRS→LRS transition. This sets a threshold stress (at 50 pA) of 36.6 MPa, which is lower than the already low pressure used earlier. This is because bond distortion requires a shear stress, which can be more efficiently generated by a uniaxial compression/tension than by a pressure in an inhomogeneous material. (Pressure cannot generate any shear stress in a homogeneous medium.) As in the pressure experiment, beam-induced resistance transition was nontransient, nondamaging (see Supporting Information, Figure S6), and one-way only: LRS devices treated identically did not switch. Since any Ga^+ accumulation on the top electrode would produce a *positive* bias whereas HRS→LRS switching under the stress-free condition requires a *negative* bias (Figure 1b), charge accumulation cannot explain the above findings. To further corroborate this, parallel experiments were performed with 30 keV electrons of the same set of current, which would produce an opposite charge accumulation. None of the devices experienced any resistance change, and all remained switchable after bombardment. This is expected: the impact pressure of electrons is a factor of $(m_{Ga}/m_e)^{1/2}$, or 356×, smaller than that of Ga^+. As an additional confirmation that a mechanical force can cause one-way, nontransient HRS→LRS switching, we observed a 100 nN load applied by a conducting atomic force microscope tip caused sudden resistance drops at a sensing voltage of 0.1 V (see data in ref 29).

Having established the mechanical and electron-occupancy nature of the electron−phonon interaction by static and quasi-static perturbations, we next address its dynamics. The time window to form the negative-U state commences after electron filling of the trap-site (happening in ~1 fs)[30] and lasts for the duration of a strong electron−phonon interaction (about one period of atomic vibration, 0.1−1 ps). Therefore, if a subpicosecond force at the short end of this period can still mechanically unravel ϕ_{ep} and cause prompt electron detrapping, it will unequivocally confirm the operation of the mechanism. (The long end, which may go well beyond 1 ps for soft phonons, is of less interest because it may be caused by thermally activated atomic or electron motion.) To provide such a fast force, we designed an experiment (Figure 3a) using the concept of the Lorentz force (Figure S7), which is a self-force acting on any circuit loop with a circulating current.

dx.doi.org/10.1021/nl501710r | *Nano Lett.* 2014, 14, 5058−5067

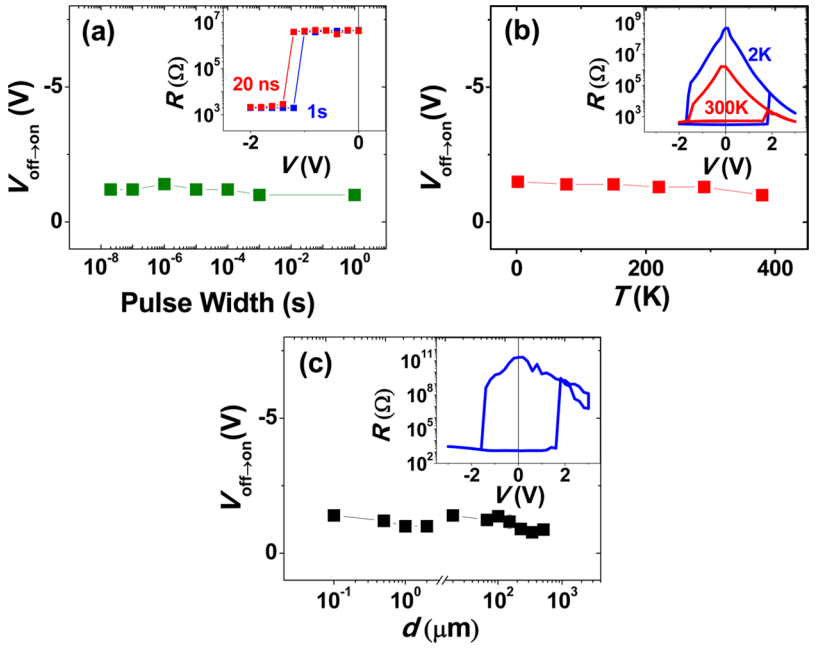

Figure 4. Invariance of threshold voltage. Threshold voltage in Si_3N_4:Cr device insensitive to (a) voltage−pulse width from 20 ns to 1 s for 2 μm devices; inset: resistance after different voltage pulses at the pulse width shown (1 s and 20 ns); (b) temperature from 2 to 300 K; inset: $R-V$ curves at 2 and 300 K; (c) device lateral size from 100 nm to 500 μm; inset: $R-V$ curve of a 100 nm device.

The key element of the experiment is to provide a 0.1 ps transient magnetic field: it will induce a current and a force that also last for 0.1 ps. In our experiment, the magnetic transient originated from a 20 GeV electron bunch (Figure 3a), which hit head-on, just once, a point on our device chip. Having a Gaussian transverse width of 35 μm and a longitudinal width of 30 μm, this bunch of about 19 billion electrons (total charge 3 nC) passed by any point in its path in a Gaussian time of 0.1 ps (FWHM = 0.235 ps). (These conditions were selected to allow the electron bunch to deposit about the same amount of area charge density, 3−5 C/m^2, as in the 30 keV Ga^+ and electron bombardment experiments.) At nearly the speed of light c, it also carried a half-cycle pulse of a (nonradiative) radial transverse electric field E (thus no voltage across the film thickness) and a circumferential magnetic induction $B = E/c$,[31−33] peaking at ∼50 T at the Gaussian edge of the bunch before decaying as a r^{-1} far-field with the radial distance r.[33,34] Since the E-field was largely screened by the top electrode but the B-field was not, the main effect on the device was exerted by a transient magnetic flux that crossed the "circuit loop" of *top-electrode→film-gap→bottom-electrode→film-gap→top-electrode* (Figure 3b, bottom panel). For this configuration, known as a planar microstrip line or patch antenna, both antenna theory[35,36] and our simulation (Figure 3b, middle panel) found a plasmonic phenomenon: an induced current (j) in the top electrode (TE) accentuated at the longitudinal edges (L), and an opposite image current (not shown) in the bottom electrode (BE) and in the heavily doped conductive Si substrate. This formed a circuit loop that activated a 0.1 ps Lorentz-force repulsion (i.e., a magnetic pressure) to push the two electrodes apart. However, because the loop is not continuous, the current discontinuity at the transverse edges (T) in the top electrode produced a set of opposite charges at T, matched by another set of opposite image charges in the bottom electrode/substrate (Figure 3b, bottom panel). Thus, the overall magnetic pressure was countered by the image-charge attractions at T. As the pressure forced the top electrode to tear, along the electrode−film interface, starting at the places where the Lorentz force was strongest (around L, especially at its center), the clamping forces counteracted to turn the partially torn top electrode into an elegant platinum "bow-tie" displayed in Figure 3b (top panel). This analysis of the mechano-plasmonic effect was corroborated by the damage contours in Supporting Information, Figure S8a, and the zone shapes of mechanical tearing: a circular zone for devices patterned as square ones (sample 1 in Figure 3a) vs a kidney-shaped zone for devices patterned as rectangles ones (sample 2 in Figure 3a), which have different clamping at different edges (Supporting Information, Figure S8b). Supplementary experiments (Supporting Information, Figure S9−10) with different substrates and electrode sizes further corroborated the above analysis: it is the repulsive Lorentz force between the induced current and its image current that caused top-electrode tearing.

With a repulsive Lorentz force between electrodes, the nanometallic film experienced a (normal) tensile stress. (When it reached the interfacial strength, typically 10−100 MPa for a metal/amorphous dielectric interface,[37,38] the top electrode may tear.) In sample 1, this tensile stress caused switching of all of the HRS devices within ∼450 μm from the electron bunch (Figure 3c). (Devices within 200 μm from the center lost the top electrode completely and were not tested.) As in Figure 2a−b, this was a one-way transition: parallel experiments on LRS devices produced no switching (Figure 3c). It was also nontransient and nondamaging: all of the switched devices—even those bow-tie ones—could be switched back as long as some part of the top electrodes was still intact (see Supporting Information, Figure S11). To reconfirm, we examined another sample (Figure 3d), with all of the devices preset to HRS and with thicker top electrodes, which did not change the induced Lorentz force but conferred higher bending rigidity thus more resistance to tearing (no visible debonding for many devices.) Indeed, its switching zone had a similar outer radius (400 μm)

dx.doi.org/10.1021/nl501710r | *Nano Lett.* 2014, 14, 5058−5067

and a smaller inner radius (~150 μm vs 200 μm). Remarkably, very near the center, which suffered the highest direct mechanical impact of electrons, there were some undamaged, unswitched HRS devices. (This was repeatedly seen in many other similar tests regardless of electrode thickness.) This is consistent with the Lorentz force mechanism because the field vanishes at the center due to radial symmetry; more importantly, it provided direct evidence that 20 GeV electron bombardment itself is not damaging at all! (These results are also consistent with the Ga-ion-induced transition, in that they both follow the same stress-dependence statistics triggering more HRS→LRS transition at a higher stress, as shown in Supporting Information, Figure S12.) In the Supporting Information, we further describe additional parallel experiments guided by scaling-law and symmetry considerations (see Methods) which ruled out all other causes (heat, electric and magnetic fields, electromagnetic pressure, impact and reflection stresses) that might have caused switching. For example, the electric field mechanism is ruled out because our device is distinctly directional having entirely different switching behavior when the voltage polarity is reversed, but the electron-bunch generated switching zone has radial symmetry despite the opposite field directions at points diagonally across from each other. Parallel experiments using a positron bunch, whose field directions are opposite to those of an electron bunch also generated the same tearing and switching patterns, further supporting the above argument. This leaves the Lorentz force as the only responsible mechanism.

The electron-bunch experiment is consistent with the electron–phonon interaction mechanism and, together, all our experiments demonstrated that forces as brief as 10^{-13} s can trigger electron detrapping causing one-way HRS→LRS transition. This implies that barrier reconfiguration, likely the rate-limiting step for electron-detrapping, can be triggered extremely fast. Therefore, one should not expect to see a rate dependence in the conventional regime of electrical testing (1 s to 1 ns), at least for the HRS→LRS transition. (Previously, one of us—B.J.C.—used 100 ps voltage pulses to demonstrate two-way switching in a nanometallic SiO_2:Pt device of 5 μm × 5 μm in size.[12]) To verify the rate-independence of the HRS→LRS transition in electrical switching, we used negative voltage pulses lasting from 1 s to 20 ns to determine the threshold voltage (pulse amplitude) V^* required for switching. (Below 20 ns, parasitic capacitance in our device causes distortion of voltage pulses.) Indeed, our 2 μm devices switched at the same V^* (Figure 4a). A similar test using positive voltage pulses confirmed that the LRS→HRS transition is also rate independent (Figure S13). In sharp contrast, over the same time span a typical memristor demands at least thrice the voltage to switch,[39−45] because of the exponential dependence of ion transport on electric field and/or local temperature (raised by Joule heating), which dictates highly nonlinear switching dynamics.[22] Consistent with the rate independency, the same switching voltage holds from 2 to 300 K (Figure 4b and Supporting Information, Figure S14). It is also independent of the device size (100 nm to 500 μm in Figure 4c) and thickness (Supporting Information, Figure S15.) Together, these results (including Figure S1) suggest that nanometallic electronic memory can operate over a very wide time/temperature/size/thickness/composition window at an essentially constant V^*, which offers simplicity and flexibility for circuit design and fabrication.

Our experiments left no doubt that electron–phonon interaction is central to nanometallic MIT,[4,11] and the transition is fundamentally different from all other stimuli-driven *reversible* MIT in the literature.[21,46−50] Without getting into the details of bipolar switching, which requires trapped electrons to be supplied from and drained to the same electrode (the lower-work-function metal in our device), a mechanistic picture of memory switching that involves a reconfigurable barrier (Figure 5) may be depicted as follows. During voltage-controlled MIT. Electron filling occurs at a threshold forward bias V^* when itinerant electrons are energetic enough to occupy a prospective negative-U trapping site, which immediately undergoes energy-lowering local bond distortion. This is the LRS→HRS transition. Under a reverse threshold bias, the distorted bond is *inelastically* restored to the original configuration by the electric force, thereby removing ϕ_{ep} stabilization, prompting the destablilized electron to detrap. This is the HRS→LRS transition. What we witnessed in our experiments was the unraveling of the negative-U state and reconfiguration of the barrier by an alternative stress mechanism: the distorted bond was mechanically restored (again *inelastically*)—hence ϕ_{ep} removed—in as fast as 0.1 ps, thereby converting the electron state from a stable negative-U state to an unstable positive-U state, which necessitated immediate (in ~1 fs) electron release and the HRS→LRS transition. Obviously, this mechanism does not suffer from the voltage–time dilemma: the switching process is fast, yet the memory is stable.

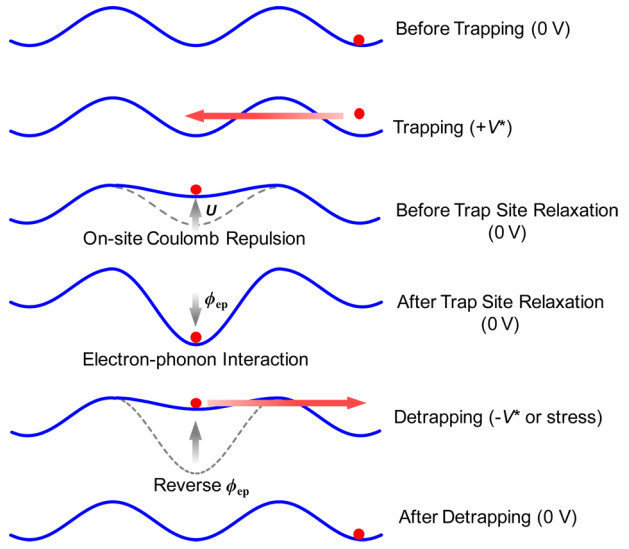

Figure 5. Electron states during trapping/detrapping. Different states of electron inside and outside a reconfigurable barrier (trap) that has two different barrier heights, one before and one after electron filling. Trapped electron energy is elevated by on-site Coulomb repulsion (positive U) and lowered by electron–phonon interaction (ϕ_{ep}), the latter may be altered by an electrical or mechanical force, causing inelastic bond distortion.

Amorphous films provide an excellent platform for the above mechanism. First, unlike the electron–phonon interaction in the global Hamiltonian of conventional MIT,[27,51−53] in amorphous films the interaction is localized to the vicinity of trapped-electrons and their surrounding over/under-bonded bonds, which correspond to a local environment that is noncompact and soft.[6] These sites are susceptible to the

dx.doi.org/10.1021/nl501710r | Nano Lett. 2014, 14, 5058−5067

applied force/stress/strain, allowing pivotal, localized electron−phonon interaction to turn on/off to reconfigure the barrier and to effect both voltage and force-triggered MIT. In the past, nonelectrically induced electronic transitions were seen in phase-change chalcogenide (Ge−Sb−Te) memory,[54−56] by photoinduced transition[57] or dislocation jamming-triggered nonmelting crystalline-to-amorphous transition.[58] Compared to these electronic transitions mediated by a bulk structural transition, nanometallic MIT involves only local structural states, not the bulk structural state. Therefore, it is far more robust and can be triggered by an atomic-scale lever of localized electron−phonon interaction. In particular, since the subpicosecond on/off of electron−phonon interactions controls nanometallic MIT, the switching voltage V^* should be independent of switching time down to ∼0.1 ps. This was partially confirmed in our electrical testing down to 20 ns and supported by our previous data down to 100 ps,[4] but future verification of voltage-driven picosecond switching is obviously welcome.

Second, the idea of electron trap through the electron−phonon coupling and negative-*U* center in our random materials is similar to the mechanism of polarons in a homogeneous material. Indeed, Anderson, who proposed the negative-*U* concept, recognized its connection to bipolarons.[59] However, switchable nanometallic materials are not polaronic materials at all! Polaron arises from electron−phonon interaction, which is a generic term in the global Hamiltonian, and a polaronic material results when the coupling is strong, which naturally occurs in a structure (e.g., S and Se) that is globally susceptible to polarization. In contrast, our switchable nanometallic materials are globally not very susceptible to polarization—their dielectric constant ε_r is ∼10 at room temperature[11] and ∼5 at low temperature.[29] However, being amorphous these materials do contain bonding/structure variations, which provide locally soft spots that are highly polarizable, especially when doped electrons are localized thereon. This contributes an "impurity" term to the local Hamiltonian, instead of a generic term to the global Hamiltonian. In practice, to find switchable nanometallicity with negative-*U* centers or local polarons, one need not search the universe of highly polarizable materials. (In such materials, our doping scheme would have led to nonswitchable polaronic conductors, not switchable nanometallic conductors.) Instead, one can simply introduce defects to relatively nonpolar materials, or make amorphous forms of relatively nonpolar materials, then dope them with electrons/holes to bond with some locally polarizable sites. As long as variations and distributions in local compositions and configurations are able to provide itinerant electrons and traps, nanometallicity and two-way switching can be realized in thin films at a certain metal composition. This explains why the switchable nanometallicity phenomenon is so ubiquitously found in so many materials (Table 1), which seem to share little commonality.

Before closing, we will make a few additional points on the electron/positron-bunch experiment.

(i) The transient stress field in the experiment is actually a stress-pulse wave because of the inertia of atoms: different parts (depths) of the film see the field at different times. (The reflected wave can be ignored because the backside of the sample is not polished.) However, since the duration of the stress pulse is of the order of the electron/positron-bunch time, switching still occurs within a subpicosecond time frame despite complicated dynamics.

(ii) The phenomenon observed is a mechano-plasmonic effect: a patch antenna of a linear dimension comparable to the beam dimension—hence the equivalent wavelength of beam's transient fields—senses a resonance-like amplified field as shown by our simulation and antenna theory.[35,36] The antenna, however, can only harnesses and amplify the far-infrared (∼30 μm) component of the field. Other field components (e.g., the high energy X-ray/bremsstrahlung radiation from the attenuating electron/positron) are not amplified.

(iii) Although photons and charged particles can generate damage on computer memories,[60] our devices are too thin for 20 GeV electrons/positrons to create many collisional cascades to directly deposit energy. Meanwhile, bremsstrahlung radiation from an ultrarelativistic electron (20 GeV $\approx 4 \times 10^4$ times the rest energy of an electron, 511 keV) is entirely forward focusing just like in a synchrotron. As a result, the radiation damage is mostly confined within a Gaussian diameter (30 μm for electrons) from the bunch—it is impossible for the radiation damage to reach out to 500 μm away to cause switching. The lack of device damage is already evident from our finding that all of the devices with intact top electrodes can still be switched at the normal voltage and current after the experiment. It is also fully corroborated by previous electron-bunch studies of magnetic switching memory.[31−33] (In these studies, a continuous thin film instead of a patterned film was used. Therefore, they lacked the mechano-plasmonic effect seen here.)

(iv) The insignificance/irrelevance of direct electron damage is further illustrated in Figure S16, which describes observations on a set of parallel experiments to "turn on/off" damage with nominally the same (within a factor of ∼2) electron/energy/momentum dosage: (a) 3 nC over 0.1 ps, (b) 1.5 nC over 0.1 ps, (c) 1.5 nC over 1 ps, and (d) 1.5 nC over 0.1 ps but with a Pt top electrode 2.5× thicker (100 nm vs 40 nm). Accordingly, one expects (a) has about twice the collision/radiation of (b) and (c), and (d) has about the same radiation but 2.5× the collision of (b) and (c). Figure S16, however, illustrates that while the visible physical damage was indeed more extended in (a) than in (b), it was minor in (d) and completely absent in (c), which is inexplicable if only dosage matters. On the other hand, the results are entirely consistent with our model and the scaling law (see Methods): (c) has a 10× weaker transient magnetic field, thus a 100× weaker Lorentz force insufficient for mechanical damage; (d) has a (15.6×) stiffer bending modulus in the Pt top electrode, thus more resistant to mechanical damage. These results reconfirmed that switching in the experiment was not caused by direct electron or radiation damage.

(v) The electron−phonon interaction can last longer than 0.1 ps. The short-time segment of the interaction is directly coupled to our 0.1 ps excitation probe, while the longer-time segment is coupled to the overtones of the 0.1 ps excitation. However, these overtones are heavily damped going away in 2−3 cycles according to our simulation. Moreover, a weak field is less effective than a strong field for switching according to Figure S16b, and a long-duration field cannot even trigger switching according to Figure S16c. Therefore, longer-time electron−phonon interactions are not important in our experiment.

(vi) Lastly, the incoming field could excite plasmons in the nanometallic film and trigger electron−phonon interaction. These plasmons are in the far-infrared regime in which the plasma frequency of a similar nanometallic film (SiO_2:Pt) lies.[3]

dx.doi.org/10.1021/nl501710r | Nano Lett. 2014, 14, 5058−5067

However, this mechanism is ruled out by the observations in Figure S16d: the thick Pt electrode configuration, which can very efficiently shield the incoming electric field, still suffers from the same extent of switching.

Finally, in retrospect, almost all memory structures must encounter the same voltage−time dilemma, but it is usually engineered around by designing a separate high-temperature (transient) route for the program/erase step—thermally assisted switching in magnetic memory,[61] melting in phase-change memory,[56] hot-filament formation in resistance memory,[22] and hot-carrier injection in flash memory[9]—albeit always at the cost of excess power consumption or damage. Our method of using electron−phonon interaction to reconfigure the barrier height is the first time that a fundamental solution has been offered to resolve the dilemma. Literally, it works as an atomic-scale lever that can be externally triggered to readjust the local barrier. In principle, such interaction can be embedded into any electronic memory structure. It already enables purely electronic nanometallic memory in random materials with wide-ranging sizes, compositions, and nanostructures. Harnessing such subpicosecond atomic levers may further enable nanoscale electron storage and gating to usher in new nanodevices with unconventional functionalities.

Methods. *Materials and Samples.*[3−5,10,11,62] Test cells were fabricated on Si/SiO_2 substrates covered by a 200-nm-thick thermally grown oxide layer. A 30 nm thick bottom electrode (Mo, Ta, $SrRuO_3$, TiN) was first deposited. Next, a layer of insulator:metal film was cosputtered onto unheated substrates using separate insulator (e.g., Si_3N_4) and metal (e.g., Cr) targets in a magnetron sputtering system. After lithography to define the top electrode pattern, a top Pt electrode was RF-sputter deposited followed by a lift-off process. To eliminate the possibility that oxide interlayer may be a factor in resistance switching, comparative studies were made using $SrRuO_3$ electrode, different Pt electrode configurations, and Si_3N_4:metal insulator:metal systems, to prevent forming such layer—they all showed the same resistance switching phenomena. Film composition was measured by energy-dispersive X-ray spectroscopy with calibration by Rutherford backscattering spectroscopy and electron energy loss spectroscopy. TEM samples were prepared by cosputtering hybrid films on carbon-coated copper grids, then directly examined by a JEOL 2010F at a 200 kV acceleration voltage.

Testing Methods. In typical electric testing, samples were placed in a probe station, and a bias voltage was applied to the top Pt electrode while the bottom electrode was grounded. Quasi-static electric characteristics were examined using a semiconductor parameter analyzer (Keithley 237). Capacitance measurements were performed using a HP4192A impedance analyzer (10^2−10^7 Hz). Capacitance data were extracted by fitting the impedance spectra using the equivalent circuit shown in the Supporting Information, Figure S17. Pulse on/off-switching characteristics were studied by providing a square-impulse-shaped voltage-pulse train of a constant width but an increasing pulse (voltage) height using an Agilent 81104A pulse generator and a Keithley 7001 digital switch box. The device resistance after each pulse was measured by a Keithley 237, and the voltage of the pulse that triggered switching was identified as the switching voltage. Switching at low temperatures was performed in a Lakeshore cryogenic probe station and a liquid He cryostat PPMS. Switching of 100 nm sized devices was tested in an atomic force microscope (AFM, Asylum MFP-3D) using a Pt/Ir-coated conducting tip connected to a homemade circuit. The same system was used to perform mechanical stressing on 2 μm sized cells, with a load controlled by the deflection of the cantilever that housed the tip, and with the cell resistance constantly monitored at +0.1 V. Isostatic pressure experiments were conducted in a hydraulic pressure vessel, with samples placed in evacuated thin elastomer bags and held at pre-determined pressure up to 1 GPa. Ion bombardment was performed in an FEI Strata DB235 which provided 30 keV Ga^+ ions with a current ranging from 10 pA to 1 nA. Electron bombardment was performed in an SEM housed in the same FEI Strata DB235. Electron-bunch shots were performed at Stanford Linear Accelerator Center (SLAC) using the FACET facility, which provided high-energy (>20 GeV), high charge (>1 nC), narrowly collimated (<50 μm), and short-duration (<1 ps) electron and positron bunches in vacuum on a pulse-by-pulse basis.[31−34]

Switching Voltages. Because the resistance of nanometallic film in the metallic state can be arbitrarily small, the on-state LRS resistance can be much higher than the actual film resistance of the device (called cell herein). The actual threshold switching voltages V^* is related to the apparent switching voltage $V_{on/off}$ by $V_{on/off} = V^* (R_{cell} + R_{BE})/R_{cell}$ (see notation in Supporting Information, Figure S17). Since the HRS resistance nearly equals the actual film resistance, the apparent first off→on switching voltage nearly equals the actual cell voltage and is the same as V^*. Further switching to LRS of a lower resistance requires more apparent voltage, but the actual cell voltage remains unchanged.[5,10,62] This information allows the determination of the ratio $(R_{cell} + R_{BE})/R_{cell}$. It also enables the determination of V^* in on→off switching. The difference between V^* of the first off→on switching and the apparent V_{off} for on→off switching depends on the sweeping voltage in the negative bias that drives the LRS state (a lower LRS resistance reached by using a larger negative bias); it is especially large in Figure S11 and 15 because a larger negative bias was used in those experiments. This aspect was modeled and discussed in detail elsewhere.[5,10,62]

Analyzing Electron/Positron-Bunch Experiments. We summarize the scaling laws assuming a very thick bottom electrode (or conducting substrate) and a top electrode thick enough to shield the direct electric field.[34−36] Conceptually it is convenient to distinguish the direct (incident) fields that travel with the electron bunch in the free space, and the induced fields due to the device (metal-on-insulator-on-metal) structure. The direct B and E scales with Q/r at large r (Q = total electron charge of electron-bunch, r = radial distance from the bunch; positron-bunch has a Q of opposite sign). The same holds for the induced fields since the Maxwell equations are linear. The Faraday emf (as a voltage V) induced by the magnetic flux is proportional to the (insulator) gap distance δ, but so is the reactance dominated by the inductance and reactance of the gap. So the induced current has no δ dependence. Likewise, it has no top-electrode thickness (t) dependence since the inductance and capacitance do not depend on t. The Lorentz force scales with (induced current),^{2} thus with $(Q/r)^2$, independent of (t, δ). Regarding time dependence, since the Faraday emf is proportional to the rate of change of magnetic flux, it scales inversely with the Gaussian time τ of the bunch. Thus the induced current also scales inversely with τ, and the Lorentz force scales inversely with τ^2. The Joule heating of the top electrode is due to the resistive part R of the impedance, which is t independent since t is thick enough. The power density, V^2/Rt, scales with $(Q/r)^2$ (δ^2/t). For heat transfer/loss

dx.doi.org/10.1021/nl501710r | Nano Lett. 2014, 14, 5058−5067

dominated by electrode's surface, the Joule heating effect scales with $(Q\delta/r)^2/t$. Regardless whether switching is induced by the Lorentz force, the direct fields, or the induced field, the switching zone radius all scales with Q, independent of (t, δ). Heat/thermal-stress induced switching gives a switching zone scaling $Q\delta/t^{1/2}$. Since the fields are vectors, there is polarity in the induced (emf) voltage, being antisymmetric with respect to the center. However, the Lorentz force is always tensile and centro-symmetric, having radial symmetry under normal bunch incidence. The bending rigidity follows a t^3 dependence, so a thicker top electrode can better resist tearing, although the Lorentz force is not affected, neither is the switching zone if induced by the Lorentz force.

■ ASSOCIATED CONTENT

Supporting Information

Figures S1 to S17. This material is available free of charge via the Internet at http://pubs.acs.org.

■ AUTHOR INFORMATION

Corresponding Author

*(I-W.C.) E-mail: iweichen@seas.upenn.edu.

Present Address

B.J.C. is currently at Department of Materials Science and Engineering, Seoul National University of Science and Technology, Seoul, Korea.

Author Contributions

X.Y. and I.T. contributed equally. X.Y. and A.B.K.C. developed the materials, X.Y. designed the ion beam experiment, I.T. and I-W.C. designed—and I.T. conducted—the electron bunch experiment, X.Y. performed pre- and postcharacterization for electron bunch experiment, X.Y., B.J.C., and A.B.K.C. performed electrical and other characterization, X.Y. and I-W.C. analyzed the data, all authors discussed the results and the manuscript.

Notes

The authors declare no competing financial interest.

■ ACKNOWLEDGMENTS

This research was supported by the US National Science Foundation (Grant No. DMR-11-04530 and DMR-14-09114, primarily, and DMR-09-07523 and DMR-11-20901, in part.) SLAC National Laboratory is supported by the US Department of Energy, Office of Basic Energy Sciences. I.T. and I-W.C. acknowledge partial support by FAME, one of six centers of STARnet, a Semiconductor Research Corporation program sponsored by MARCO and DARPA.

■ REFERENCES

(1) Anderson, P. W. *Phys. Rev.* **1958**, *109*, 1492−1505.
(2) Egami, T. *Nat. Nanotechnol.* **2011**, *6*, 199−200.
(3) Chen, A. B. K.; Kim, S. G.; Wang, Y.; Tung, W.-S.; Chen, I. W. *Nat. Nanotechnol.* **2011**, *6*, 237−241.
(4) Choi, B. J.; Chen, A. B. K.; Yang, X.; Chen, I. W. *Adv. Mater.* **2011**, *23*, 3847−3852.
(5) Chen, A. B. K.; Choi, B. J.; Yang, X.; Chen, I. W. *Adv. Funct. Mater.* **2012**, *22*, 546−554.
(6) Egami, T. *Prog. Mater. Sci.* **2011**, *56*, 637−653.
(7) Schroeder, H.; Zhirnov, V. V.; Cavin, R. K.; Waser, R. *J. Appl. Phys.* **2010**, *107*, 054517.
(8) Liu, Z. T.; Lee, C.; Narayanan, V.; Pei, G.; Kan, E. C. *IEEE Trans. Electron Devices* **2002**, *49*, 1606−1613.
(9) Liu, Z. T.; Lee, C.; Narayanan, V.; Pei, G.; Kan, E. C. *IEEE Trans. Electron Devices* **2002**, *49*, 1614−1622.
(10) Yang, X.; Chen, I. W. *Sci. Rep.* **2012**, *2*, 744.
(11) Yang, X.; Choi, B. J.; Chen, A. B. K.; Chen, I. W. *ACS Nano* **2013**, *7*, 2302−2311.
(12) Choi, B. J.; Torrezan, A. C.; Norris, K. J.; Miao, F.; Strachan, J. P.; Zhang, M.-X.; Ohlberg, D. A. A.; Kobayashi, N. P.; Yang, J. J.; Williams, R. S. *Nano Lett.* **2013**, *13*, 3213−3217.
(13) Hou, T.-H.; Lee, C.; Narayanan, V.; Ganguly, U.; Kan, E. C. *IEEE Trans. Electron Devices* **2006**, *53*, 3095−3102.
(14) Hou, T.-H.; Lee, C.; Narayanan, V.; Ganguly, U.; Kan, E. C. *IEEE Trans. Electron Devices* **2006**, *53*, 3103−3109.
(15) Lee, C. H.; Meteer, J.; Narayanan, V.; Kan, E. C. *J. Electron. Mater.* **2005**, *34*, 1−11.
(16) Sawa, A. *Mater. Today* **2008**, *11*, 28−36.
(17) Sawa, A.; Fujii, T.; Kawasaki, M.; Tokura, Y. *Appl. Phys. Lett.* **2006**, *88*, 232112.
(18) Oshima, H.; Miyano, K.; Konishi, Y.; Kawasaki, M.; Tokura, Y. *Appl. Phys. Lett.* **1999**, *75*, 1473−1475.
(19) Watanabe, Y.; Bednorz, J. G.; Bietsch, A.; Gerber, C.; Widmer, D.; Beck, A.; Wind, S. J. *Appl. Phys. Lett.* **2001**, *78*, 3738−3740.
(20) Meijer, G. I.; Staub, U.; Janousch, M.; Johnson, S. L.; Delley, B.; Neisius, T. *Phys. Rev. B* **2005**, *72*, 155102.
(21) Asamitsu, A.; Tomioka, Y.; Kuwahara, H.; Tokura, Y. *Nature* **1997**, *388*, 50−52.
(22) Yang, J. J.; Strukov, D. B.; Stewart, D. R. *Nat. Nanotechnol.* **2013**, *8*, 13−24.
(23) Wong, H. S. P.; Lee, H.-Y.; Yu, S.; Chen, Y.-S.; Wu, Y.; Chen, P.-S.; Lee, B.; Chen, F. T.; Tsai, M.-J. *Proc. IEEE* **2012**, *100*, 1951−1970.
(24) Strukov, D. B.; Snider, G. S.; Stewart, D. R.; Williams, R. S. *Nature* **2008**, *453*, 80−83.
(25) Kwon, D. H.; Kim, K. M.; Jang, J. H.; Jeon, J. M.; Lee, M. H.; Kim, G. H.; Li, X. S.; Park, G. S.; Lee, B.; Han, S.; Kim, M.; Hwang, C. S. *Nat. Nanotechnol.* **2010**, *5*, 148−153.
(26) Valov, I.; Linn, E.; Tappertzhofen, S.; Schmelzer, S.; Hurk, J.; Lentz, F.; Waser, R. *Nat. Commun.* **2013**, *4*, 1771.
(27) Imada, M.; Fujimori, A.; Tokura, Y. *Rev. Mod. Phys.* **1998**, *70*, 1039−1263.
(28) Tokura, Y.; Nagaosa, N. *Science* **2000**, *288*, 462−468.
(29) Yang, X. *Resistance switching devices based on amorphous insulator-metal thin films*. Ph.D. Dissertation, University of Pennsylvania, Philadelphia PA, 2014.
(30) Blochl, P. E.; Stathis, J. H. *Phys. Rev. Lett.* **1999**, *83*, 372−375.
(31) Back, C. H.; Allenspach, R.; Weber, W.; Parkin, S. S. P.; Weller, D.; Garwin, E. L.; Siegmann, H. C. *Science* **1999**, *285*, 864−867.
(32) Tudosa, I.; Stamm, C.; Kashuba, A. B.; King, F.; Siegmann, H. C.; Stohr, J.; Ju, G.; Lu, B.; Weller, D. *Nature* **2004**, *428*, 831−833.
(33) Stamm, C.; Tudosa, I.; Siegmann, H. C.; Stohr, J.; Dobin, A. Y.; Woltersdorf, G.; Heinrich, B.; Vaterlaus, A. *Phys. Rev. Lett.* **2005**, *94*, 197603.
(34) Gamble, S. J.; Burkhardt, M. H.; Kashuba, A.; Allenspach, R.; Parkin, S. S. P.; Siegmann, H. C.; Stoehr, J. *Phys. Rev. Lett.* **2009**, *102*, 217201.
(35) Leone, M.; Singer, H. L. *IEEE Trans. Electromagn. Compat.* **1999**, *41*, 418−424.
(36) Bernardi, P.; Cicchetti, R. *IEEE Trans. Electromagn. Compat.* **1990**, *32*, 98−105.
(37) Gupta, V.; Yuan, J.; Pronin, A. *J. Adhes. Sci. Technol.* **1994**, *8*, 713−747.
(38) Gupta, V.; Yuan, J. *J. Appl. Phys.* **1993**, *74*, 2397−2404.
(39) Schindler, C.; Staikov, G.; Waser, R. *Appl. Phys. Lett.* **2009**, *94*, 072109.
(40) Menzel, S.; Waters, M.; Marchewka, A.; Boettger, U.; Dittmann, R.; Waser, R. *Adv. Funct. Mater.* **2011**, *21*, 4487−4492.
(41) Cao, M. G.; Chen, Y. S.; Sun, J. R.; Shang, D. S.; Liu, L. F.; Kang, J. F.; Shen, B. G. *Appl. Phys. Lett.* **2012**, *101*, 203502.
(42) Yu, S.; Wu, Y.; Wong, H. S. P. *Appl. Phys. Lett.* **2011**, *98*, 103514.

(43) Strachan, J. P.; Torrezan, A. C.; Miao, F.; Pickett, M. D.; Yang, J. J.; Yi, W.; Medeiros-Ribeiro, G.; Williams, R. S. *IEEE Trans. Electron Devices* **2013**, *60*, 2194−2202.
(44) Ielmini, D.; Nardi, F.; Balatti, S. *IEEE Trans. Electron Devices* **2012**, *59*, 2049−2056.
(45) Medeiros-Ribeiro, G.; Perner, F.; Carter, R.; Abdalla, H.; Pickett, M. D.; Williams, R. S. *Nanotechnology* **2011**, *22*, 095702.
(46) Limelette, P.; Georges, A.; Jerome, D.; Wzietek, P.; Metcalf, P.; Honig, J. M. *Science* **2003**, *302*, 89−92.
(47) Cao, J.; Ertekin, E.; Srinivasan, V.; Fan, W.; Huang, S.; Zheng, H.; Yim, J. W. L.; Khanal, D. R.; Ogletree, D. F.; Grossmanan, J. C.; Wu, J. *Nat. Nanotechnol.* **2009**, *4*, 732−737.
(48) Liu, M. K.; Pardo, B.; Zhang, J.; Qazilbash, M. M.; Yun, S. J.; Fei, Z.; Shin, J.-H.; Kim, H.-T.; Basov, N.; Averitt, R. D. *Phys. Rev. Lett.* **2011**, *107*, 066403.
(49) Ueno, K.; Nakamura, S.; Shimotani, H.; Ohtomo, A.; Kimura, N.; Nojima, T.; Aoki, H.; Iwasa, Y.; Kawasaki, M. *Nat. Mater.* **2008**, *7*, 855−858.
(50) Liu, M.; Hwang, H. Y.; Tao, H.; Strikwerda, A. C.; Fan, K.; Keiser, G. R.; Sternbach, A. J.; West, K. G.; Kittiwatanakul, S.; Lu, J.; Wolf, S. A.; Omenetto, F. G.; Zhang, X.; Nelson, K. A.; Averitt, R. D. *Nature* **2012**, *487*, 345−348.
(51) Egami, T.; Ishihara, S.; Tachiki, M. *Science* **1993**, *261*, 1307−1310.
(52) Egami, T.; Billinge, S. J. L. *Prog. Mater. Sci.* **1994**, *38*, 359−424.
(53) Weber, F.; Rosenkranz, S.; Castellan, J. P.; Osborn, R.; Hott, R.; Heid, R.; Bohnen, K. P.; Egami, T.; Said, A. H.; Reznik, D. *Phys. Rev. Lett.* **2011**, *107*, 107403.
(54) Siegrist, T.; Jost, P.; Volker, H.; Woda, M.; Merkelbach, P.; Schlockermann, C.; Wuttig, M. *Nat. Mater.* **2011**, *10*, 202−208.
(55) Zhang, W.; Thiess, A.; Zalden, P.; Zeller, R.; Dederichs, P. H.; Raty, J. Y.; Wuttig, M.; Bluegel, S.; Mazzarello, R. *Nat. Mater.* **2012**, *11*, 952−956.
(56) Raoux, S.; Ielmini, D.; Wuttig, M.; Karpov, I. *MRS Bull.* **2012**, *37*, 118−123.
(57) Kolobov, A. V.; Krbal, M.; Fons, P.; Tominaga, J.; Uruga, T. *Nat. Chem.* **2011**, *3*, 311−316.
(58) Nam, S.-W.; Chung, H.-S.; Lo, Y. C.; Qi, L.; Li, J.; Lu, Y.; Johnson, A. T. C.; Jung, Y.; Nukala, P.; Agarwal, R. *Science* **2012**, *336*, 1561−1566.
(59) Anderson, P. W. *Phys. Rev. Lett.* **1975**, *34*, 953−955.
(60) Ziegler, J. F.; Lanford, W. A. *Science* **1979**, *206*, 776−788.
(61) Prejbeanu, I. L.; Kerekes, M.; Sousa, R. C.; Sibuet, H.; Redon, O.; Dieny, B.; Nozieres, J. P. *J. Phys.: Condens. Matter* **2007**, *19*, 165218.
(62) Yang, X.; Chen, A. B. K.; Choi, B. J.; Chen, I. W. *Appl. Phys. Lett.* **2013**, *102*, 043502.